Chapter 9

# Three-Dimensional Visualization and Quantification of Structural Fibres for Biomedical Applications

Magnus B. Lilledahl, Gary Chinga-Carrasco and Catharina de Lange Davies

Additional information is available at the end of the chapter

http://dx.doi.org/10.5772/55891

## 1. Introduction

Confocal laser scanning microscopy (CLSM) combined with the broad range of new fluorescent probes, has become an indispensable tool in basic and applied research within a variety of areas. Extending CLSM to multiphoton microscopy (MPM) and nonlinear optical microscopy (NLOM) opens further possibilities. MPM can be used to increase the penetration into the sample, and is thus ideal for thick samples and *in-vivo* imaging. In this chapter we describe briefly the principles of MPM and non-linear imaging techniques such as second harmonic generation (SHG) and Coherent anti-Stokes Raman scattering (CARS) microscopy. These imaging techniques are especially useful to study structural molecules such as collagen and cellulose. Image analysis is crucial to extract quantitative information about various parameters, for instance the structure of molecules in the sample. Such quantitative information can be used as input parameters in mathematical models describing mechanical properties of tissue. Here we describe 3D Fourier transformation to obtain structural information, gradient techniques, used to characterize the orientation, and distance transforms to measure the thickness of fibres. Additionally, biomedical applications of collagen and cellulose imaging will be presented.

## 2. Confocal laser scanning and multiphoton microscopy

CLSM is widely used to image cells *in vitro*. Relatively thick samples up to approximately 50 μm can be imaged. By using a confocal pinhole, out-of-focus scattered light is rejected and depth selective imaging is achieved. The absorption and scattering of photons through the

tissue limit the corresponding penetration depth. Furthermore, the confocal pinhole rejects scattered light from the focal plane, reducing the detection efficiency. Extending CLSM to MPM makes it possible to penetrate further into the sample, and imaging several hundred μm, has been reported [1].

Two-photon excitation arises from the simultaneous absorption of two photons and requires a high photon density. The excitation is thus intrinsically confocal and no pinhole in front of the detector is required. To obtain a sufficient number of photons in the focal volume, high power, pulsed femtosecond IR lasers are used. The absorption cross section depends on the square of the excitation intensity, and absorption occurs only in the focal volume [2], [3]. Thus, no absorption or photo-bleaching occurs above or below the focal plane, as illustrated in Figure 1. The reduced absorption of photons through the tissue and the use of IR excitation light which is less scattered than visible light, is responsible for the possibility of imaging deeper into the thick sample. Furthermore, the detection of emitted photons can be more efficient than in CLSM as no pinhole is needed in front of the detector and thereby more scattered photons can reach the photomultiplier tubes. 3D imaging of thick specimens, based on 3D reconstruction of 2D optical slices, is superb in MPM compared to CLSM, as no bleaching occurs outside the focal plane. 3D imaging several hundred μm into the sample is regularly reported and imaging down to 1 mm in brain tissue has been achieved [1] - [4]. Most fluorescent organic dyes, quantum dots, and reporter proteins can be excited in a two-photon process, although the absorption spectra are very different from single photon excitation spectra [5]. The excitation is followed by emission of photons from the same excited state as after single photon excitation, thus the emitted fluorescence has the same spectrum in the two cases.

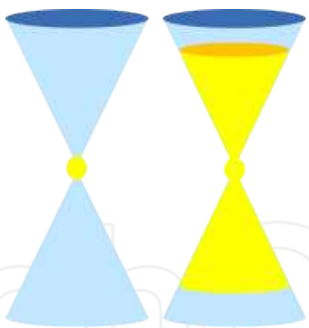

**Figure 1.** Schematic illustration of the difference between one- and two-photon absorption. On the left is two-photon absorption which only occurs in the small focal volume. On the right, the one-photon absorption occurs above and below the focal plane.

The pulsed IR laser can be used for SHG, another non-linear process. SHG requires that the second order optical susceptibility is non-zero, thus occurring only in non-centrosymmetric molecules [6]. Two photons combine their energy and emit a photon with exactly twice the energy of the two incoming photons, or equivalently, at half the wavelength [7]. The interaction is illustrated in the Jablonski diagram in Figure 2. Thus, placing a narrow bandpass filter at half the wavelength of the excitation light in front of the detector, the SHG signal is easily detected. It should be emphasized that in the SHG process no energy is lost and SHG does not

http://dx.doi.org/10.5772/55891

involve an excited state, as opposed to the two-photon excitation fluorescence where some of the incoming energy is lost during relaxation of the excited state. Consequently, SHG does not involve excitation of molecules and no phototoxicity occurs. The SHG signal is polarization sensitive and its intensity depends on the angle between the fibres and the polarization of the excitation light. Therefore, polarization sensitivity studies of SHG from tissues can provide information on the fibre organization. Furthermore, the SHG signal is anisotropic and can be detected in both the forward and backscattered direction. The SHG signal in the forward direction is generally dominating, but if the size of the scattering structures along the optical axis is less than the wavelength, the intensity of the backscattered signal will be equal or even larger than the forward signal [8].

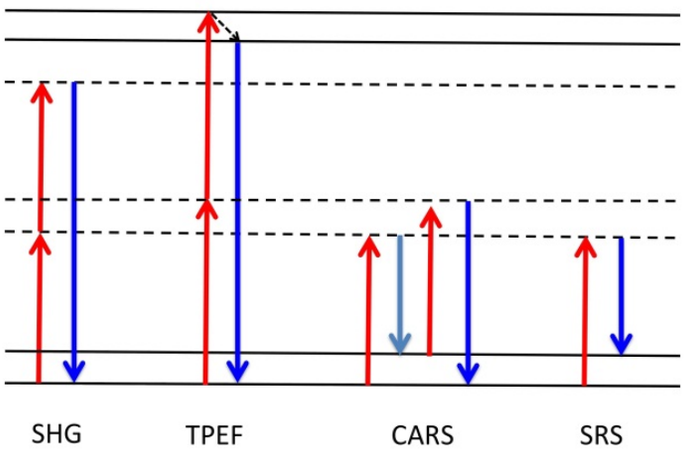


**Figure 2.** Jablonski diagram illustrating several nonlinear processes. SHG: Two photons are converted to a single photon with twice the energy, corresponding to half the wavelength. TPEF: Two photons are absorbed simultaneously to excite a molecular energy state which can emits fluorescene as if excited by a single molecule. CARS: Three beams interact with a vibrational mode to emit photons at slightly longer wavelengths. SRS: Two beams interact with a vibrational level to transfer energy from one beam to the other.

A major advantage of SHG is that no exogenous labeling of the sample is needed. This label-free technique can be used to image materials with a non-centrosymmetric molecular organization. Examples of such molecules are protein fibres such as collagen, microtubules and actomyosin, as well as cellulose. Combining SHG, two photon excitation fluorescence (TPEF) and conventional CLSM makes it possible to obtain information in the same sample of various molecular and structural constituents (see applications below).

A recent addition to the family of nonlinear optical microscopy is coherent anti-Stokes Raman scattering (CARS) and stimulated Raman scattering (SRS) microscopy [9], [10]. These techniques allow for imaging contrast based on molecular vibrational states, similar to information derived from spontaneous Raman spectroscopy. These methods are slightly more technically complex as two pulsed lasers, temporally and spatially overlapped, must be employed. In CARS, the detection is at a different wavelength than the excitation lasers, so filter-based detection is used. For SRS, the signal is actually a decrease or increase in the laser light intensity

so detection of the weak signal in the presence of the laser noise is challenging. A technique called modulation transfer is used where one of the laser beams is modulated and a corresponding modulation in the signal is detected using a lock-in amplifier. CARS and SRS are mainly used for imaging lipids which give a very strong signal, but recent work have shown the potential for imaging other biologically relevant molecules, *e.g.* cellulose [11]. CARS and SRS, together with TPEF and SHG provide the opportunity to image a wide range of structural fibres without exogenous stains. This means that dynamic process (*e.g.* in tissue engineering or biomass processing) may be monitored over time.

## 3. NLOM and structural fibres

Structural fibres are abundant in nature. They provide support for the cells to develop complex organs. Not only do the fibres provide mechanical support, but they are also modifiers for cellular behaviour. They control the diffusion of signalling molecules and act as signalling molecules themselves, for example through mechanobiological transduction.

NLOM is especially useful when imaging structural fibres in biological thick samples. The thicker 3D volumes generated will facilitate the subsequent analysis of 3D structural information. Also, being able to perform optical sectioning through thicker sections than in CLSM, fewer serial sections have to be cut mechanically, which reduces workload and potential for sectioning artefacts. When using traditional fluorophores for providing imaging contrast, the main advantage of nonlinear microscopy is the reduced out-of-focus bleaching and the availability of non-descanned detection.

However, the main advantage of NLOM for imaging structural properties lies in the possibility of using endogenous signals from the molecule in question to generate contrast in the image. This is highly advantageous as there are limitations in quantitation caused by uneven labelling or fading of the fluorescence. Furthermore, since the signal is generated from the molecule itself, and not some fluorescent molecule attached to it, a range of optical signals (polarization, spectral, lifetime) can be used to extract even sub-resolution information about the molecule. For example, SHG has been used to measure the helical pitch angle of myosin and collagen with a high degree of accuracy [12]. Fortunately, nature has also provided bright nonlinear endogenous signals from several highly relevant structural molecules, e.g. collagen [7] with SHG, elastin [13] with TPEF and cellulose [11] with CARS.

### 3.1. Collagen

Collagen is the most abundant protein in the extracellular matrix (ECM) in animals. Collagen forms fibres with high tensile strength and thus accounts for much of the mechanical strength of tissue. Collagen exists in many different varieties but the main common feature is a polypeptide with repeating sequences of three amino acids. Typically, every third amino acid is glycine. The repeating sequence can thus be described as gly-X-Y where the amino acids in the X and Y positions vary. Three of these polypeptides then form a triple stranded helix to create a collagen molecule. Various combinations of the three strands yields different collagen

http://dx.doi.org/10.5772/55891

types which are denoted by roman numerals (I,II, III etc.). Some of these types have a molecular structure which causes them to aggregate into even larger structures called collagen fibrils (~20-500 nm in diameter), and the fibrils form fibre collagens (e.g. type I and II) (~500-3000 nm in diameter). Due to their semi-crystalline ordering and non-centrosymmetric structure of the collagen molecule, these fibrils are efficient emitters of SHG. In addition to the SHG intensity, the full tensor nature of the second order susceptibility and the ratio of forward to backscattered light may be used to extract sub-resolution information about the molecules. Several works have illustrated how the orientation of the collagen molecules can be determined from a single pixel and how the forward/backward scattering ratio can be used to determine the size and sub-resolution structure of collagen fibrils [8].

### 3.2. Elastin

Elastin fibres are aggregates of monomers of the elastin molecule, which are covalently bound through cross-links. These cross-links are very flexible so that the polymer can stretch quite significantly without breaking, thus giving rise to the elasticity of tissue. Elastin has a strong TPEF (probably linked to the molecular cross-links). Elastin is found in many important organs e.g. skin, arteries and some types of cartilage. Imaging of elastin fibres is especially striking in elastic arteries where such imaging has been used for biomechanical applications and atherosclerosis research [13].

### 3.3. Cellulose

Cellulose is the main component of the cell wall of green plants. In vascular plants, cellulose is a major component of the structural fibres that provide mechanical stability and are responsible for transporting water and nutrients. Cellulose, lignin and hemicellulose are the major components of wood fibres, or tracheids. The cellulose molecules form the elementary fibrils, which have been reported to be the structural unit of natural cellulose, with a diameter of 3.5 nm [14] - [16]. The cellulosic components of a wood fibre wall structure are the cellulose molecule, the elementary fibril, the microfibril, the macrofibril and the lamellar membrane [15]. The mentioned cellulosic constituents compose various layers of the fibre wall structure, including the primary wall (P) and secondary walls (S1, S2 and S3) [17].

## 4. Sample preparation

For nonlinear microscopy one typically wants to cut samples which are much thicker than samples used for conventional histology. This is to take advantage of the 3D imaging capability of the techniques. We have successfully cut fixed and embedded sections of breast tissue with a rotary vibratome up to 100 microns. The challenge with thicker samples is to remove all the paraffin, but we found that this is usually not a problem if slightly longer incubation for removal of paraffin is used.

For samples which are not embedded, a vibratome is good choice for cutting sections of desired thickness. Here the challenge is on the other end of the scale, that is, creating thin samples. We

have found that sections down to 40 microns of unfixed and unembedded cartilage are easily cut. Thinner samples are not necessary, as imaging down to 40 micron is straightforward and typically thicker sections can be cut. A vibratome requires a certain rigidity of the sample, but we have found that cartilage is an ideal sample to cut with this technique.

Cryosections are also possible. There is some concern that the freezing procedure might cause structural changes but this depends heavily on the structure that is to be imaged. For example, cryosections of collagen fibres in cartilage have been shown to be well preserved. This might also be the case for other structural fibres due to their inherent mechanical strength [30]. For other, more delicate structures (e.g. cell structures), preparation artefacts and lost morphology might be a concern.

Of course, in addition to the endogenous signal, tissues might also be stained with various fluorochromes to access the distribution of other molecules of interest. For thick sections, the additional stain penetration is an issue. This is highly dependent on the size of the staining molecule and the type of tissue. For fixed and embedded samples from breast tissue we have been able to stain nuclei with DAPI down to about 50 micron, yielding striking images of the cellular distribution relative to the collagen network imaged with SHG (Figure 3).

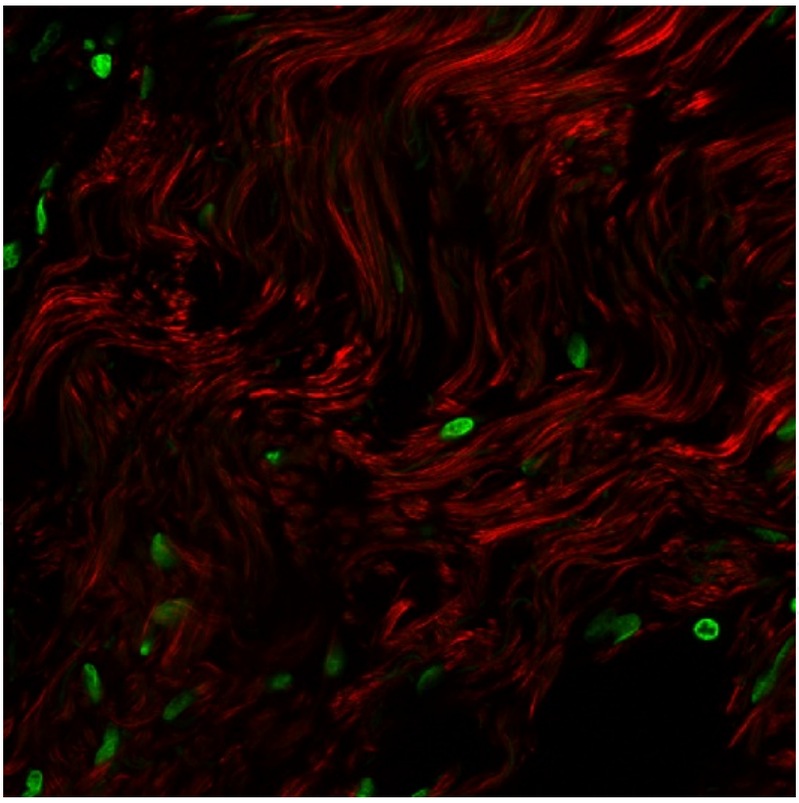

**Figure 3.** Breast cancer tissue imaged with SHG (red) to visualize collagen structure and TPEF (green) of DAPI stained cells. The collagen structure may serve as a prognostic marker for the degree of malignancy.

Since one of the main advantages of NLOM is the 3D imaging capability, enhancing this feature is often desirable. This leads to the concept of optical clearing. By substituting the water in the

http://dx.doi.org/10.5772/55891

tissue with some other compound which has a refractive index comparable to cells and the collagen fibres, the scattering is greatly reduced. We have seen up to a two-fold increase in the penetration depth, based on this technique (typically 50 % increase) (see Figure 4). A useful compound is glycerol. It is nontoxic and has little interaction with the samples. Furthermore, the refractive index of glycerol can be tuned by using various mixing ratios of water and glycerol, to optimize the effect of the clearing.

## 5. Image analysis

The organization of structural fibres has a wide variety of effects on the biology of the components it supports. The primary property is structural, *i.e.* keeping the cells in appropriate relative positions. They also comprise a major part of the mechanical properties of tissue through load bearing, distribution of loads and mechanotransduction. It has also become clear recently, that structural fibres also have a profound biological role, acting both as a signalling molecule themselves, as well as determining the diffusion of other signalling molecules [18].

To be able to incorporate these parameters into mathematical models for biological systems, quantitative data needs to be derived from the images. Several image analysis methods have been developed for this purpose and a few of the most common ones are presented in this chapter.

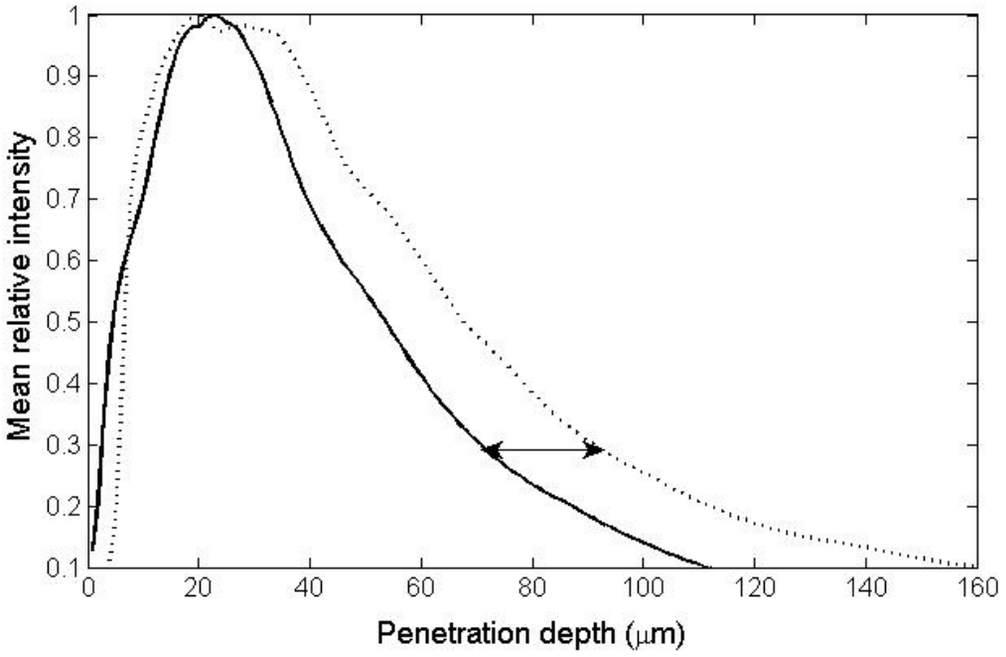


**Figure 4.** Change in penetration depth due to optical clearing. Mean SHG signal in an image frame as a function of depth for uncleared sample (solid line) and cleared with 70% glycerol (dashed line)

### 5.1. Fourier analysis

The linear arrangement of fibres in many types of structures and the resulting periodicity of the fibres in the direction perpendicular to the fibres immediately leads to the idea of using the Fourier transform of the image to determine the direction of the fibres (Figure 5) [19] - [21]. Even though the idea is simple, aligned fibres rarely yields a perfectly sinusoidal signals and significant processing is necessary to extract the desired information.

The one dimensional discrete Fourier transform $F(k)$ of a signal $f(x)$ of length N is given by

$$F(k) = \sum_{x=0}^{N-1} f(x) e^{-\frac{i2\pi kx}{N}} \tag{1}$$

where $k$ is the spatial frequency of the signal. A periodic signal will give an impulse response in the frequency spectrum at the frequency of the periodic signal. Due to the linearity of the transform, a signal consisting of many frequency components will yield distinct peaks in the Fourier space. As the Fourier transform is complex, the power spectrum (magnitude of the Fourier spectrum) is typically employed for interpretation of the signals. In graphical representations of the power spectrum the DC component is usually shifted to the center of the image. An important point to note is that even though the Fourier transform is linear (Fourier transform of a sum of signals is equal to the sum of the Fourier transform of the individual signals) this is not true for the power spectrum. Hence, care should be taken when interpreting the power spectrum as a sum of individual components.

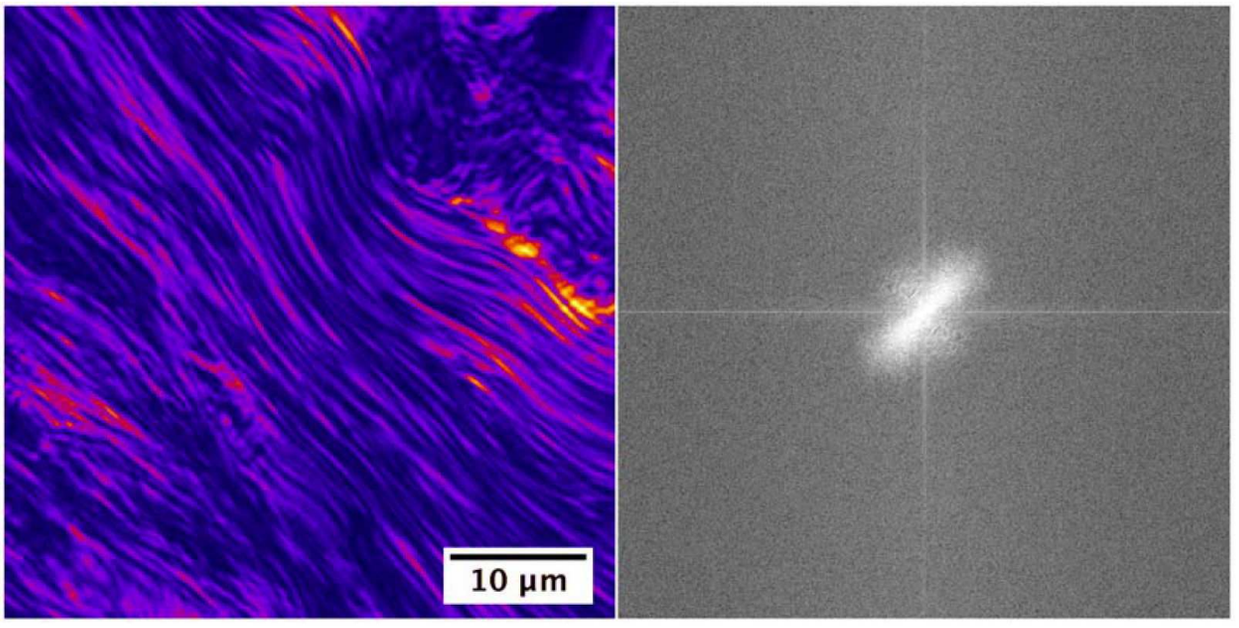


**Figure 5.** Left) SHG image of collagen fibres from chicken cartilage. Pseudocolours have been applied for better visualization. Right) The corresponding Fourier transform of the SHG image.

http://dx.doi.org/10.5772/55891

The most common way to interpret Fourier transform images is to assume that the frequency components are distributed on an ellipse (or ellipsoid in three dimensions). The long axis is perpendicular to the direction of the fibre, which corresponds to strong frequency components (periodicity) in this direction. Again, it must be noted that an ellipse is not the resulting frequency pattern of a specific ordered fibre distribution (as seen in Figure 5, right), but rather represents some of the inherent variability of the systems which are analyzed. There are several methods for fitting an ellipsoid to data. See for example [34].

To avoid aliasing in the image due to edge effects, it is important to add a windowing function to the image. The edge effect can be seen in Figure 5 (right), as straight lines through the center of the image. These are however easily removed by a windowing function. Several options are possible, with the Blackman-Harris function and the Hann window being popular candidates [19].

Also, as can be seen in Figure 5 (right) the pure Fourier image is quite noisy, and there is a lot of signal which is not relevant to the structure of interest. Before extracting the directional information it is often necessary to filter the data to get a good result. Typically, a band pass filter can be employed which lets through the frequencies associated with the fibrils. The approach removes random high frequency components and low frequency components which represent slow variations in intensity across the image. The frequency limits of the band pass filter must be determined from the size of the structures of interest. An example can be found in [34].

Due to the linearity of sums (or integrals for the continuous case) used in the Fourier transform, the extension of the one dimensional transform to two, three and higher dimensions is trivial. Hence, the 3D image volumes generated by CLSM and NLOM may be analyzed by the 3D Fourier transform. An important point to keep in mind when analyzing 3D volumes with the Fourier transform, is that the point spread function of the microscope is not equal in all three directions. This will cause an elongation of signals in the z-direction, thereby reducing the higher order frequency components in this direction. This must be taken into account when trying to extract quantitative information.

### 5.2. Gradient techniques

During the years several methods for characterization texture have been developed, including autocorrelation, Fourier transform, gradient analysis and quadtree decomposition. Gradient analysis is an interesting approach, as this technique can be applied for estimating the orientation of fibrous structure, *i.e.* collagen and cellulose nanofibrils (Figure 6). Several gradient definitions have been proposed [22]. However, Sobel operators are particularly attractive due to the noise enhancing effect of derivatives [23]. Examples are the orientation of short-fibre composites [24] and actin fibres in cytoskeletal structures [25].

A relatively simple approach for quantification of structural orientation has been implemented in the SurfCharJ plugin for ImageJ [26]. The plugin plots the frequency of azimuthal angles for estimating the preferred orientation of a given structure. In addition, an estimation of the structural orientation based on the mean resultant vector is provided [27].

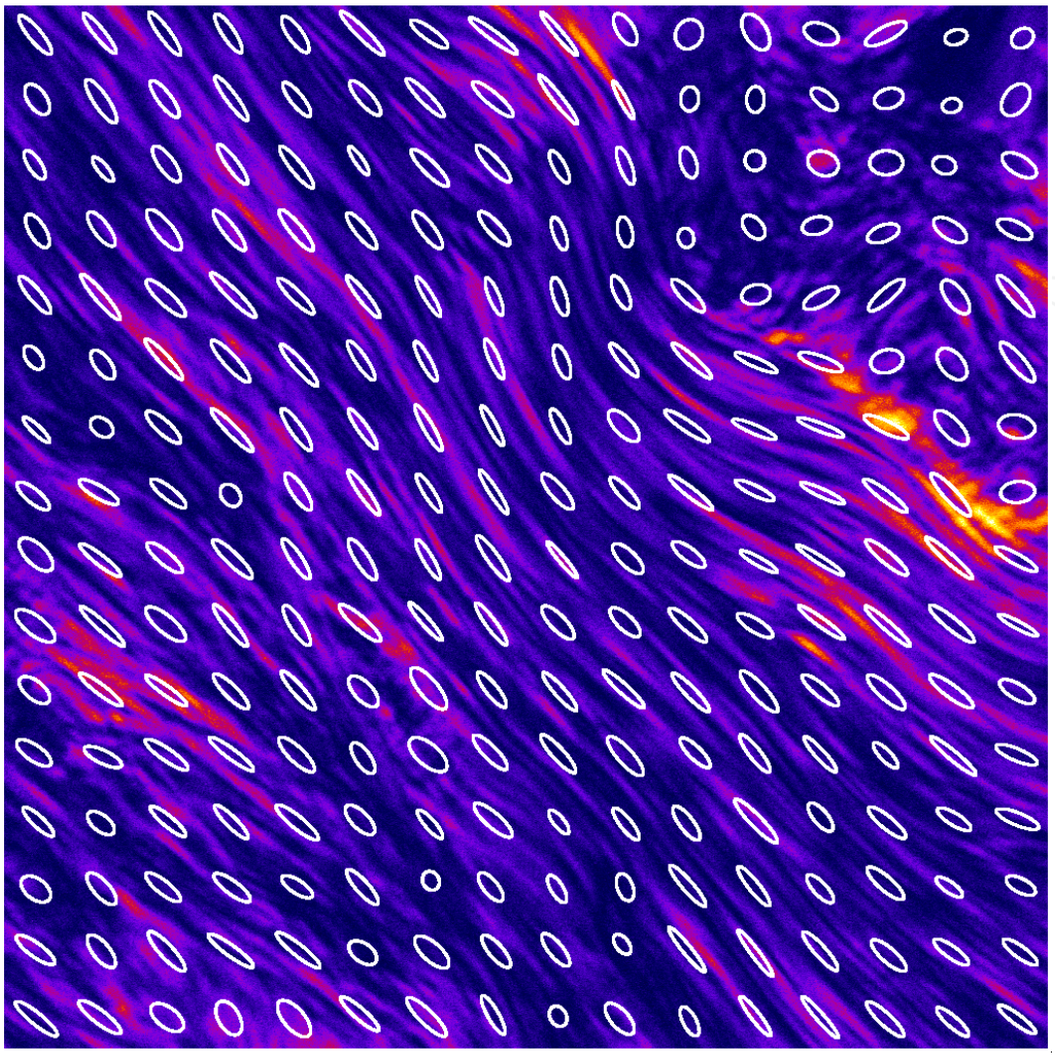

**Figure 6.** SHG image of collagen fibres analyzed with gradient techniques. Ellipses have been superimposed to exemplify the local direction of the fibres.

### 5.3. Distance transforms

A distance transform converts a binary image to a grey level image, where all pixels have a value corresponding to the distance to the nearest feature pixel [28]. The lateral size of fibrous structures can thus be estimated, provided that the previous segmentation is adequate (Figure 7). Some common metrics for estimating the distance between pixels are the City-block (*Eq. 2)*, Chessboard (*Eq. 3)* and Euclidean distance (*Eq. 4)*:

$$d_b = |x_1 - x_2| + |y_1 - y_2| \tag{2}$$

$$d_c = [\,|x_1 - x_2|,\ |y_1 - y_2|\,] \tag{3}$$

$$d_e = \sqrt{(x_1 - x_2)^2 + (y_1 - y_2)^2} \tag{4}$$

http://dx.doi.org/10.5772/55891

where $d_b$, $d_c$, and $d_e$ represent the distance between pixel $(x_1, y_1)$ and pixel $(x_2, y_2)$ as computed by the City-block, Chessboard and Euclidean distance transforms, respectively.

A distance transform can be efficiently applied for estimating the thickness of collagen and cellulose fibres, as exemplified in Figure 7.

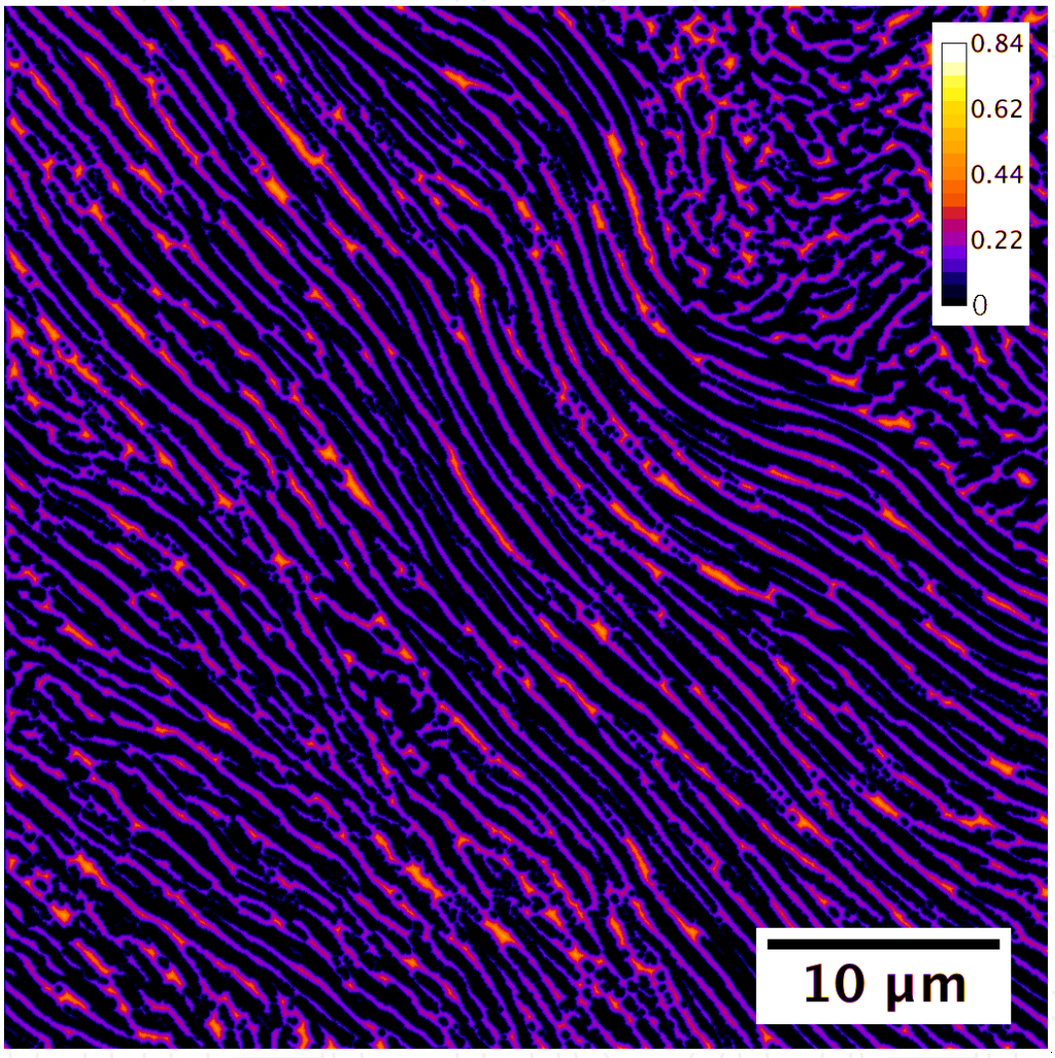


**Figure 7.** SHG image of collagen fibres. The distance transform map exemplifies the approximate lateral dimensions of the fibres. The calibration and scale bars are given in micrometers.

## 6. Image acquisition in NLOM

Optimizing a nonlinear optical system is demanding, especially for more complex techniques like SRS and CARS. We will in this section address a few points, which must be considered. To improve the generated signal, the first step is to maximize the photon density, while keeping the average power constant. As the femtosecond laser pulses undergo significant dispersion

as they propagate through the optics of the microscope, pre-chirping the laser pulse is necessary to achieve a transform limited pulse. The most recent generation of Ti:Sapphire lasers have such a system integrated.

The next thing to consider is the objective, which should have a high numerical aperture (NA). High NA usually means large magnification which is typically a disadvantage, as a large field of view is also desirable. The latest high-end objectives can achieve about 20-25x magnification with a NA of around unity. The objective should also have good transmission and achromaticity in the NIR spectra region. Another important point to consider, especially when imaging in deep tissue, is that there might be significant spherical aberration. Therefore a correction collar might be useful.

Often the excitation light wavelength is governed by the fluorophore used. However, if the application allows a choice (e.g. with SHG), longer wavelengths are scattered less and will result in deeper penetration depths [29]. It should also be kept in mind that many molecules, especially structural ones which have a preferred orientation, have a highly polarization dependent response [6]. To avoid bias in the images due to this effect, circularly polarized excitation should be used or ideally a variable polarization of the laser beam and an analyzer on the detection side. This polarization dependence can also be used to derive additional information, as already explained.

## 7. Applications

Collagen, ubiquitous in the vertebrate body, has been imaged in a host of different tissues using SHG. Several proof-of-principle studies exist, but there are few that actually have used the signals to derive clinical, biological or quantitative data. However, as the instrumentation becomes more user-friendly and wide spread, we will likely see an even further increase in the use of NLOM for more clinical and biological applications. We will here present a few model systems where nonlinear and confocal microscopy can provide relevant structural information.

### 7.1. Cartilage

Cartilage consists of a highly hydrated (70% water) proteoglycan gel, which is reinforced with collagen fibres, primarily type II collagen (Figure 8). The tissue provides both distribution of load across the joint surface, and a low friction surface for joint articulation. Degradation and traumatic injuries to cartilage are major health challenges, especially with an increasingly old and obese population. Osteoarthritis (OA), characterized by a degradation of the collagen matrix is one such disease. The development of OA is linked both to biological and biomechanical causes, and there is interplay between these effects. To understand the biological effects, the biomechanical effects of OA must be understood. The biomechanics is tightly connected to the collagen matrix which not only imparts tensile strength to the tissue, but also affects diffusion and fluid flow, which affects the biomechanical response. SHG, being able to

http://dx.doi.org/10.5772/55891

characterize the collagen structure in great detail, is an ideal tool for generating high fidelity structural input parameters for biomechanical models.

SHG from cartilage was first described by Yeh et al. which imaged canine cartilage and showed that several structural features could be discerned [31]. Mansfield used polarization sensitive SHG to derive directional information from the cartilage [32], [33]. We have taken a different approach and used Fourier transforms of images where individual fibrils are resolved to extract 3D structural information. As a model tissue, we use excised cartilage from chicken. These samples were sectioned in 100 μm sections using a vibratome, placed on objective slides and subsequently imaged. We have shown that this information can be directly employed in biomechanical models to improve the fidelity of such models. This has been applied to assess how the tissue responds to mechanical loading and how the mechanical properties are altered as the tissue undergoes pathological changes [34].

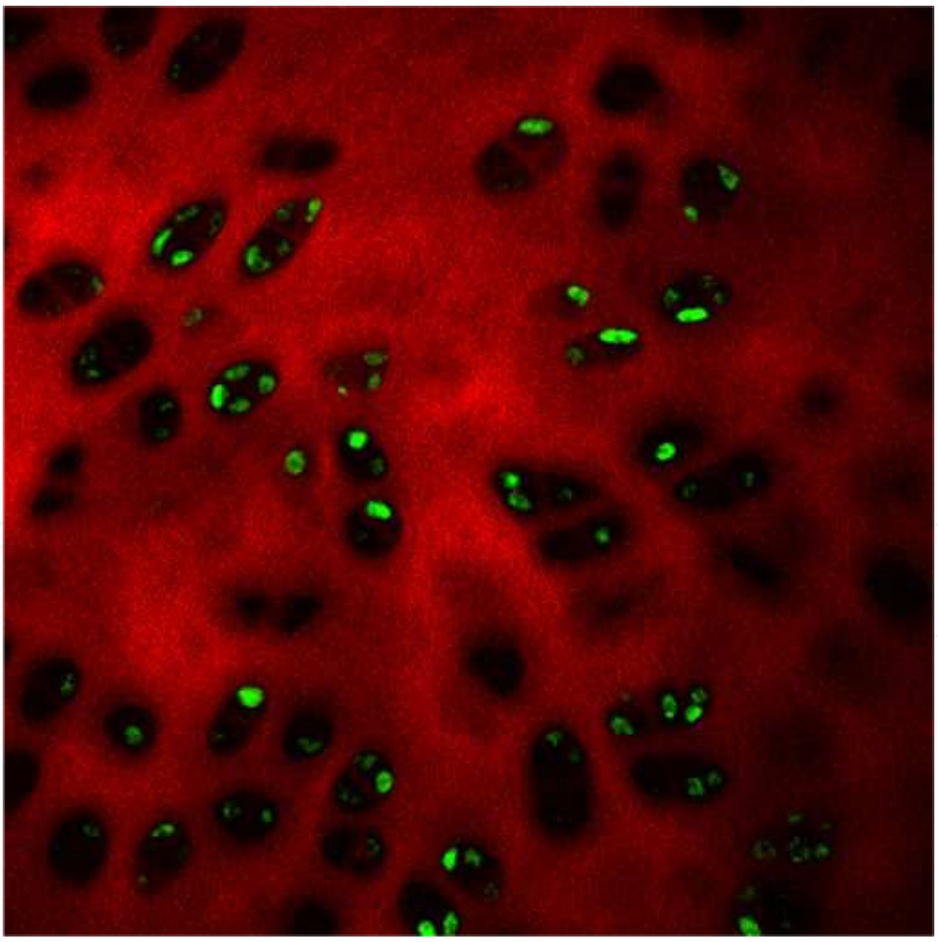

**Figure 8.** Collagen and chondrocytes in the transitional layer of cartilage imaged with SHG (red) and TPEF (green), respectively.

### 7.2. Atherosclerosis

Atherosclerosis is a disease characterized by an inflammatory process where monocytes are recruited to the vessel and differentiated into macrophages (Figure 9). As the diseases progress, a necrotic core of lipids and cellular debris develops, which is covered by a collagenous cap holding the pathological tissue, called a plaque. It is believed that a large part of heart attacks are caused by the rupture of these plaques which exposes the blood stream to the thrombogenic substances in the plaque and causes an occlusion of the artery. Plaques, which are prone to rupture, are denoted vulnerable plaques.

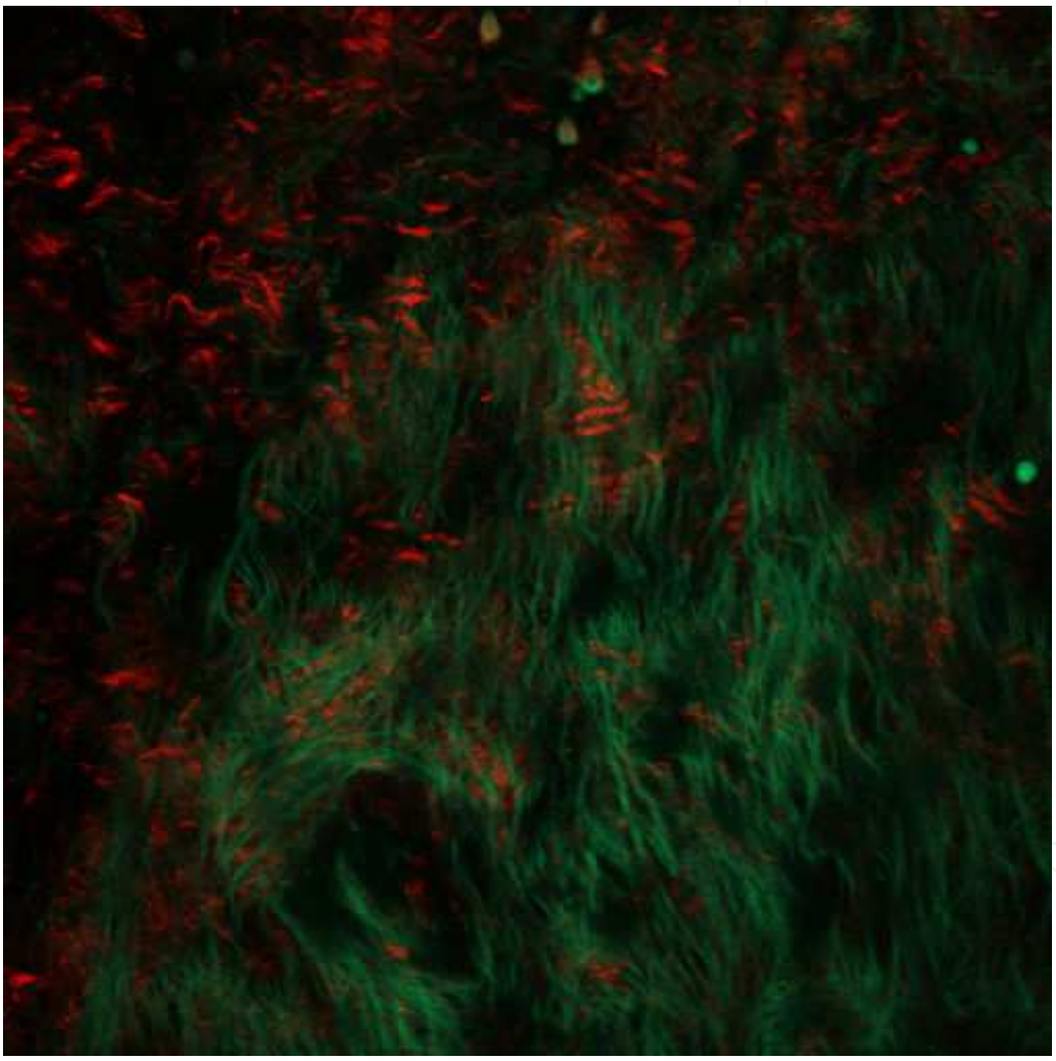

**Figure 9.** Collagen and elastin in arterial wessel imaged with SHG (red) and TPEF (green), respectively

There are several highly important molecules related to atherosclerosis, which can be imaged label-free using NLOM. Firstly, the collagenous cap of the atherosclerotic plaques are easily imaged with SHG. The cap is a very important structure as it is really the mechanical degradation (through the degradation of collagen by matrix metalloproteinases) of this cap, which ultimately leads to the disruption. The elastic fibres of the media are readily imaged using

http://dx.doi.org/10.5772/55891

TPEF. As the plaque remodels and develops, smooth muscle cells are recruited through the media and any disruption or increased permeability may be monitored using TPEF. Using samples from human autopsies, we have studied how different plaque structures can be characterized using NLOM [17]. In this study, unprepared samples were placed on a cover glass and imaged from the lumen side. Hence, similar data could potentially be extracted using an *in-vivo* fibre based probe. Finally CARS and SRS are ideal for imaging the lipids in the necrotic core. They can be used to differentiate between many different lipid types (triglycerides, cholesterol and its esters) as well as the degree of crystallinity through SHG [13], [35]. The development of cholesterol crystals have been linked to an increased vulnerability of the plaques.

### 7.3. Drug delivery through the extracellular matrix

In cancer therapy, encapsulation of drugs into nanoparticles is a promising strategy to enhance the accumulation of the drugs in tumor tissue and reduce the exposure to healthy tissue (Figure 10). This is due to the leaky blood vessels in tumor tissue, allowing the extravasation of nanoparticles from the blood vessels to the ECM, whereas the nanoparticles are constrained to the vessel in normal tissue. However, a major obstacle for successful delivery of drugs and nanoparticles to cells is the poor penetration through the ECM. The ECM consists of a network of the structural protein collagen embedded in a gel of hydrophilic glycosaminoglycans. Both the hydrophilic gel and the collagen network represent a hindrance for delivery of nanoparticles. To study the barrier represented by the collagen network, imaging of the collagen by the SHG signal gives valuable information to improve drug delivery [36], [37]. Especially intravital microscopy of tumors growing in dorsal window chambers on the back of athymic mice combined with SHG provides a valuable tool to image collagen fibres *in vivo* (Figure 10). The structure of the collagen network can be characterized by various parameters such as the anisotropy parameter [38], the second order nonlinear optical susceptibility [39], fibre angle [40], skewness and entropy [41].

### 7.4. Cellulose nanofibrils

Being the most abundant organic polymer on Earth, cellulose generates a wide range of research worldwide. Additionally, cellulose is exploited industrially, including various applications, *e.g.* a major component in paper, as thickeners in tooth paste, in paints and a series of pharmaceutical applications. During the last decades major research has been performed on the production and applications of cellulose nanofibrils [42] - [45]. This nanostructural component is commonly produced from wood pulp fibres, but other agricultural waste products have also been assessed as potential raw materials for their production [46].

Recently, cellulose nanofibrils from wood have been proposed as a major component of cryo-gels for wound healing applications. Cryo-gels based on cellulose are macro-porous and have wall structures composed of nano-sized fibrils (Figure 11) [47]. Due to this multi-dimensionality, proper characterization of porous cellulose nanofibril structures is demanding. Considering the limitations with respect to resolution, and provided an adequate preparation of the sample, the walls of cellulose macro-porous structures can be visualized. Two-photon

fluorescence microscopy may be used for this purpose by staining the cellulose with for example calcofluor white. The 3D capabilities provided by nonlinear microscopy can provide enhanced understanding of the water retaining properties of cryo-gels, which is most important (Figure 12). CARS has also been used for imaging cellulose fibres and using polarization sensitive measurements, sub-resolution about molecular orientation may be derived [11]. This label-free imaging technique is thus expected to be useful for characterizing samples, which are meant for future use (quality assurance) as well as for monitoring the development of nanofibrils as they are processed using various chemical pre-treatments [48].

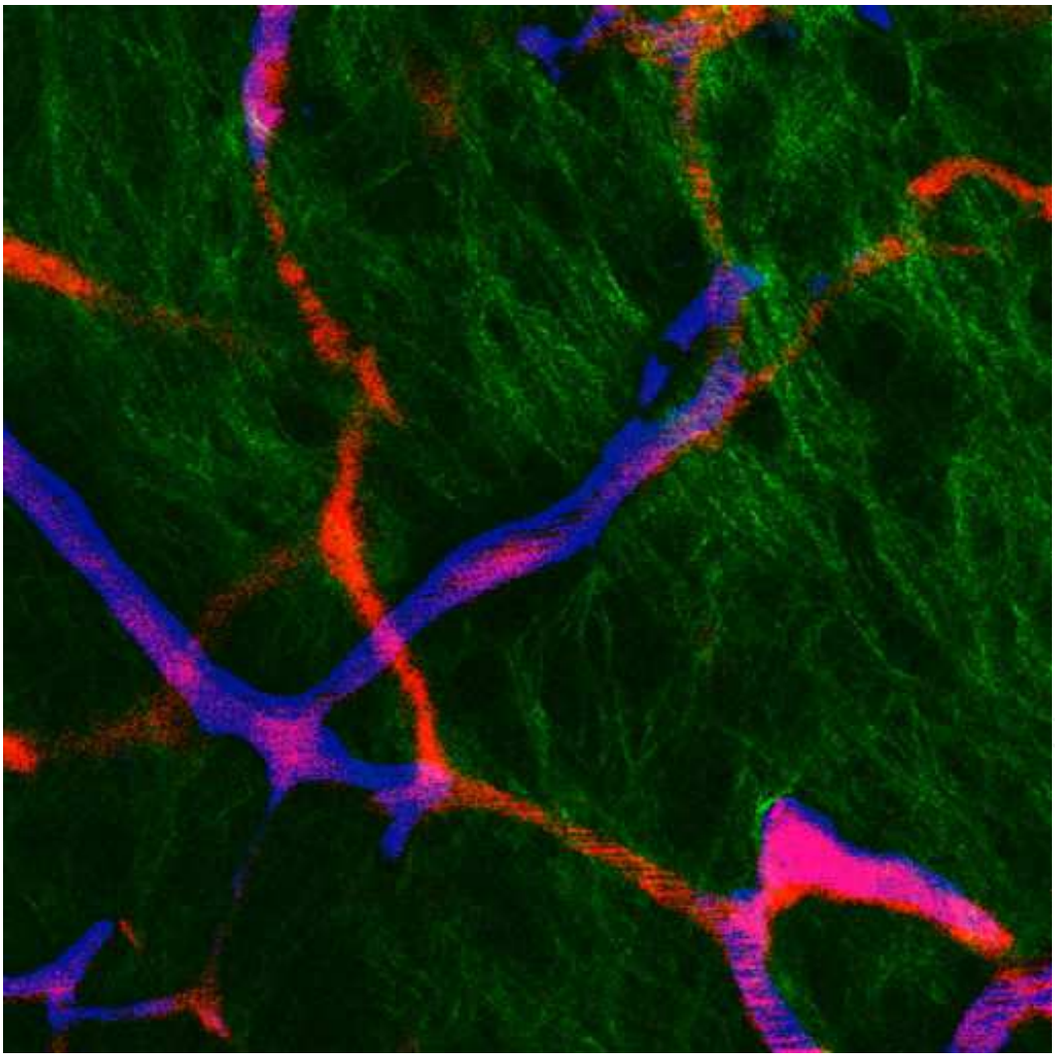

**Figure 10.** Tumor tissue growing in a dorsal window chamber. Collagen visualized by SHG (green), blood vessels (red) and nanoparticles (blue).

http://dx.doi.org/10.5772/55891

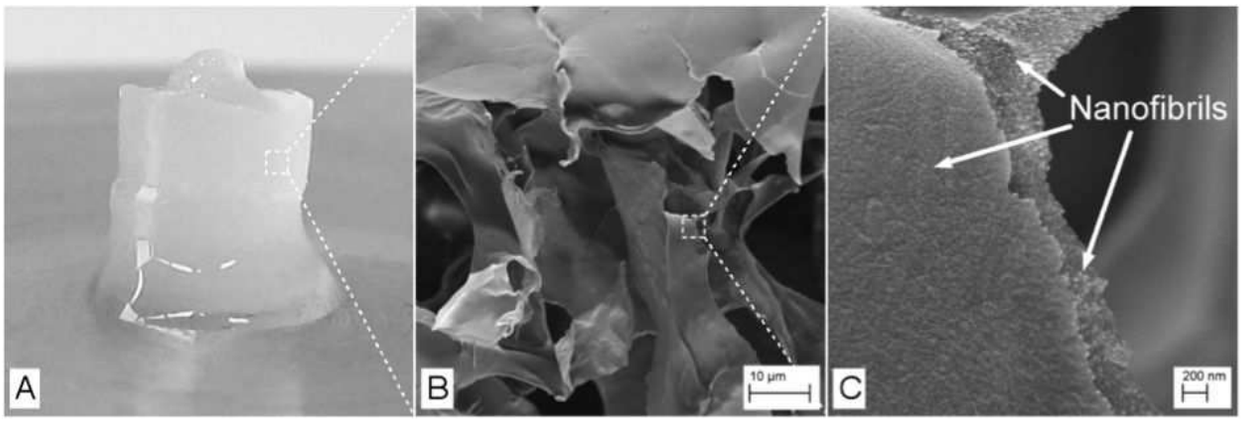


**Figure 11.** A) Elastic cryo-gel prepared from cross-linked cellulose nanofibrills. B) The macro-porous structure is exemplified. C) The nanofibrils are visualized. Reproduced from [47].

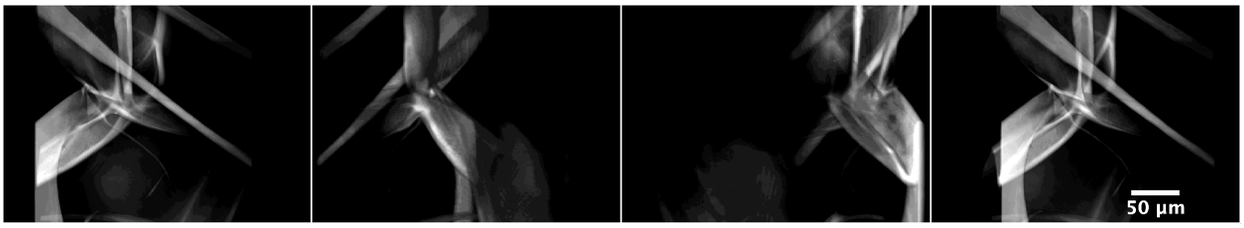


**Figure 12.** Three-dimensional rendering of a macro-porous cellulose structure in a wet state, observed from different angles. The sample was stained with Calcofluor White (CFW) before imaging.

## 8. Conclusion

Structural fibres are ubiquitous in biology were they play a wide array of roles. They provide support to the cells to develop complex organs. Not only do the fibres provide mechanical support but they are also modifiers of cellular behaviour, as they control the diffusion of signalling molecules and act as signalling molecules themselves, for example through mechanobiological transduction. The structural fibres included in this book chapter are cellulose and collagen fibres, from plant and animal tissue, respectively. We have in this chapter shown that nonlinear optical microscopy is an important extension of basic CLSM providing both label-free and three dimensional imaging. Adequate image acquisition and relevant image analysis techniques widen the possibilities for structural characterization. The ability to adequately characterize structural fibres thus expands our understanding of biological processes, which can be most important in medical applications.

## Acknowledgements

This work has been funded in part by the NanoHeal project - Bio-compatible cellulose nanostructures for advanced wound healing applications, Grant 219733. Anna Bofin provided the breast cancer samples. The images of the breast cancer samples were acquired by Anders Brabrand and Ian Kariuki.

## Author details

Magnus B. Lilledahl[1], Gary Chinga-Carrasco[2] and Catharina de Lange Davies[1]

1 Dept. of Physics, Norwegian University of Science and Technology, Trondheim, Norway

2 Paper and Novel Materials, PFI, Trondheim, Norway

## References

[1] Brown, E. B.; Campbell, R. B.; Tsuzuki, Y.; Xu, L.; Carmeliet, P.; Fukumura, D.; Jain, R. K. *Nat Med* 2001, *7*, 864.

[2] Helmchen, F.; Denk, W. *Nature Mehods* 2005, *2*, 932.

[3] Patterson, G. H.; Piston, D. W. *Biophys. J.* 2000, *78*, 2159.

[4] Theer, P.; Hasan, M. T.; Denk, W. *Optics Letters* 2003, *28*, 1022.

[5] Xu, C.; Zipfel, W.; Shear, J. B.; Williams, R. M.; Webb, W. W. *P Natl Acad Sci USA* 1996, *93*, 10763.

[6] Stoller, P.; Kim, B.-M.; Rubenchik, A. M.; Reiser, K. M.; Da Silva, L. B. *J Biomed Opt* 2002, *7*, 205.

[7] Campagnola, P. J.; Loew, L. M. *Nat Biotech* 2003, *21*, 1356.

[8] Williams, R. M.; Zipfel, W. R.; Webb, W. W. *Biophysical journal* 2005, *88*, 1377.

[9] Zumbusch, A.; Holtom, G. R.; Xie, X. S. *Physical Review Letters* 1999, *82*, 4142.

[10] Freudiger, C. W.; Min, W.; Saar, B. G.; Lu, S.; Holtom, G. R.; He, C.; Tsai, J. C.; Kang, J. X.; Xie, X. S. *Science* 2008, *322*, 1857.

[11] Zimmerley, M.; Younger, R.; Valenton, T.; Oertel, D. C.; Ward, J. L.; Potma, E. O. *J Phys Chem B* 2010, *114*, 10200.

[12] Psilodimitrakopoulos, S.; Santos, S. I. C. O.; Amat-Roldan, I.; Thayil, A. K. N.; Artigas, D.; Loza-Alvarez, P. *J Biomed Opt* 2009, *14*, 014001.

[13] Lilledahl, M. B.; Davies, C. d. L.; Haugen, O. A.; Svaasand, L. O. *J Biomed Opt* 2007, *12*, 044005.

[14] Frey-Wyssling, A. *Science* 1954, *119*, 80.

[15] Meier, H. *Pure and applied chemistry* 1962, *5*, 37.

[16] Heyn, A. N. J. *Journal of Ultrastructure Research* 1969, *26*, 52.

[17] Brandström, J. *IAWA Journal* 2001, *22*, 333.

[18] Vogel, W. F. *Eur J Dermatol* 2001, *11*, 506.

[19] Chaudhuri, S.; Nguyen, H.; Rangayyan, R. M.; Walsh, S.; Frank, C. B. *Biomedical Engineering, IEEE Transactions on* 1987, *BME-34*, 509.

[20] Xia, Y.; Elder, K. *J Microsc-Oxford* 2001, *204*, 3.

[21] Brezinski, M. E.; Tearney, G. J.; Bouma, B. E.; Izatt, J. A.; Hee, M. R.; Swanson, E. A.; Southern, J. F.; Fujimoto, J. G. *Circulation* 1996, *93*, 1206.

[22] Tovey, N.; Krinsley, D. *Bulletin of Engineering Geology and the Environment* 1992, *46*, 93.

[23] Gonzalez, R.; Woods, R. E. *Digital Image Processing*; Addison-Wesley Publishing Company, Inc., 1993.

[24] Gadala-Maria, F.; Parsi, F. *Polymer Composites* 1993, *14*, 126.

[25] Yoshigi, M.; Clark, E. B.; Yost, H. J. *Cytometry Part A* 2003, *55A*, 109.

[26] Chinga, G.; Johnsen, P. O.; Dougherty, R.; Berli, E. L.; Walter, J. *Journal of Microscopy* 2007, *227*, 254.

[27] Curray, J. R. *Bulletin of the american association of petroleum geologists* 1953, *40*, 2440.

[28] Borgefors, G. *Computer Vision, Graphics, and Image Processing* 1986, *34*, 344.

[29] Kobat, D.; Horton, N. G.; Xu, C. *J Biomed Opt* 2011, *16*, 106014.

[30] Brockbank, K.; MacLellan, W.; Xie, J.; Hamm-Alvarez, S.; Chen, Z.; Schenke-Layland, K. *Cell and Tissue Banking* 2008, *9*, 299.

[31] Yeh, A. T.; Hammer-Wilson, M. J.; Van Sickle, D. C.; Benton, H. P.; Zoumi, A.; Tromberg, B. J.; Peavy, G. M. *Osteoarth Cartilage* 2005, *13*, 345.

[32] Mansfield, J.; Yu, J.; Attenburrow, D.; Moger, J.; Tirlapur, U.; Urban, J.; Cui, Z. F.; Winlove, P. *J Anat* 2009, *215*, 682.

[33] Mansfield, J. C.; Winlove, C. P.; Moger, J.; Matcher, S. J. *J Biomed Opt* 2008, *13*, 044020.

[34] Lilledahl, M. B.; Pierce, D. M.; Ricken, T.; Holzapfel, G. A.; de Lange Davies, C. *Medical Imaging, IEEE Transactions on* 2011, *30*, 1635.

[35] Suhalim, Jeffrey L.; Chung, C.-Y.; Lilledahl, Magnus B.; Lim, Ryan S.; Levi, M.; Tromberg, Bruce J.; Potma, Eric O. *Biophysical Journal* 2012, *102*, 1988.

[36] Brown, E.; McKee, T.; diTomaso, E.; Pluen, A.; Seed, B.; Boucher, Y.; Jain, R. K. *Nature Medicine* 2003, *9*, 796.

[37] McKee, T. D.; Grandi, P.; Mok, W.; Alexandrakis, G.; Insin, N.; Zimmer, J. P.; Bawendi, M. G.; Boucher, Y.; Breakefield, X. O.; Jain, R. K. *Cancer Research* 2006, *66*, 2509.

[38] Hompland, T.; Erikson, A.; Lindgren, M.; Lindmo, T.; de Lange Davies, C. *J Biomed Opt* 2008, *13*, 054050.

[39] Erikson, A.; Örtegren, J.; Hompland, T.; Davies, C. d. L.; Lindgren, M. *J Biomed Opt* 2007.

[40] Erikson, A.; Andersen, H. N.; Naess, S. N.; Sikorski, P.; Davies, C. d. L. *Biopolymers* 2008, *89*, 135.

[41] Erikson, A.; Tufto, I.; Bjønnum, A. B.; Bruland, Ø. S.; De Lange Davies, C. *Anticancer Res* 2008, *28*, 3557.

[42] Turbak, A. F.; Snyder, F. W.; Sandberg, K. R. *Microfibrillated cellulose, a new cellulose product: properties, uses, and commercial potential*, 1983.

[43] Siró, I.; Plackett, D. *Cellulose* 2010, *17*, 459.

[44] Klemm, D.; Kramer, F.; Moritz, S.; Lindström, T.; Ankerfors, M.; Gray, D.; Dorris, A. *Angewandte Chemie International Edition* 2011, *50*, 5438.

[45] Chinga-Carrasco, G. *Nanoscale Research Letters* 2011, *6*, 417.

[46] Alila, S.; Besbes, I.; Vilar, M. R.; Mutjé, P.; Boufi, S. *Industrial Crops and Products* 2013, *41*, 250.

[47] Syverud, K.; Kirsebom, H.; Hajizadeh, S.; Chinga-Carrasco, G. *Nanoscale Research Letters* 2011, *6*, 1.

[48] Saar, B. G.; Zeng, Y.; Freudiger, C. W.; Liu, Y.-S.; Himmel, M. E.; Xie, X. S.; Ding, S.-Y. *Angewandte Chemie International Edition* 2010, *49*, 5476.